Available online at www.sciencedirect.com
ScienceDirect
Physica A 371 (2006) 226–248
PHYSICA A
www.elsevier.com/locate/physa

Morphological transitions of capillary rise in a bundle of two and three solid parallel cylinders

D. Lukáš[a,*], J. Chaloupek[a], E. Košťáková[a], N. Pan[b], I. Martinková[c]

[a]*Technical University of Liberec, Hálkova 6, Liberec 1, 461 17, Czech Republic*
[b]*Division of Textiles, Biological and Agricultural, Engineering Department, University of California, Davis, CA 95616, USA*
[c]*Internationales Hochschulinstitut, Zittau, Markt 23, 02763 Zittau, Germany*

Received 17 September 2005; received in revised form 3 April 2006
Available online 12 May 2006

Abstract

Morphological transitions here refer to the liquid-body instability of capillary rise as the spacing among cylinders changes and are studied in this paper with both theoretical analysis and experimental verifications for systems composed of two and three equidistant and parallel cylinders systems. The theory predicts cross-sectional shapes of the bounded liquid body in a bundle of cylinders, when gravity is neglected, as a function of the cylinder–cylinder separation, contact angle and the Harkinson/spreading parameter. All these morphological transitions in turn reveal the hysteresis mechanisms in the processes.

The problems dealt with cover the full spectrum of wetting behaviors, from complete wetting, to partial wetting and up to the super-hydrophobic surfaces, characterized by the corresponding contact angles and the Harkinson spreading parameters. Unlike the wetting over a flat solid surface, the wetting of bundles of cylinders exhibits much more complexities because of the geometrical curvatures and shapes involved. Various transitions and their criteria are described and derived, extensive parametric studies then followed, and the hysteresis during the transitions is analyzed. Some experimental verifications are provided at the end.

Keywords: Morphological transitions; Capillary liquid columns; Complete wetting and super-hydrophobic surface; Transition hysteresis

1. Introduction

In a series of papers published in 1960s, Princen considered the capillary rise between two vertical cylinders [1], and subsequently three-, four-, and multi-cylinder systems [2]. The last paper in the series [3] was devoted to the study of the equilibrium configurations of limited amounts of liquid in horizontal cylinder assemblies, where gravitational effects were neglected. All Princen's works were focused on partial wetting cases where the contact angles ranged within the interval $0^\circ < \theta < 180^\circ$, i.e. the Harkinson parameter, defined as $S = \gamma_{SV} - \gamma_{SL} - \gamma$, $0 > S > -2\gamma$, where γ is the liquid surface tension, and γ_{SV}, γ_{SL} are the solid–gas and solid–liquid surface tensions.

*Corresponding author.
E-mail address: david.lukas@tul.cz (D. Lukáš).

0378-4371/$ - see front matter © 2006 Elsevier B.V. All rights reserved.
doi:10.1016/j.physa.2006.04.045

Princen stated in Ref. [3] that a liquid column between two horizontal cylinders can no longer maintain its circular cross-section as soon as the separation between the cylinders exceeds certain critical value; the liquid then acquires a body shape similar to that of an unduloid on a single cylinder. This abrupt change in the liquid-body shape is called a morphological transition. It was also found [3] that the liquid columns in bundles of more than two cylinders will undergo two successive morphological transitions, again depending on the cylinder–cylinder separation. If the spacing is small enough, the liquid bridges only between each pair of adjacent cylinders (forming multi-liquid columns), with the central channel left open. If the distance increases to a critical value, the liquid fills completely the open channel among the cylinders (turning into a single column). Further increasing of the distance reduces the liquid shape back to unduloid.

Such transitions to unduloids are often taken as a manifestation of the Rayleigh instability [4,5], a phenomenon commonly occurring in liquid and cylindrical solid systems. However, the Rayleigh instability is in fact the result, not the cause, of the morphology transitions, as shown for example in the experiments of both Princen's [3] and this present work. We thus believe that, when analyzing the initiation of morphological transitions between various types of long liquid columns, it is mistaken to take the Rayleigh instability into account. Rayleigh instability is mainly attributed to the tendency of a liquid body to form unduloids when spacing among cylinders is too big so the influence of the triplet solid–liquid–gas lines that maintain the integrity of the liquid is insufficient to prevent the unduloidal instability.

The above-described liquid morphology transition has become an interest in several recent studies. For instance, Lenz and Lipowsky have shown in Ref. [4] that liquid droplets on circular planar surfaces and liquid channels on striped domains exhibit several distinct morphologies and may undergo morphological transitions between different states (homogeneous pattern, heterogeneous patterns, and film states) depending on the volume of the liquid phase.

Gau et al. [6] have presented another study on the behaviors of liquid micro-channels on structured surfaces on a plate consisting of hydrophilic stripes periodically adhered on a hydrophobic substrate. The liquid channels formed in between the strips go through shape instability at certain amount of adsorbed liquid volume, from a homogeneous state with a spatially constant cross-section to a state with a single bulge.

Swain and Lipowsky have studied wetting phenomena for a slab geometry consisting of a wetting phase confined between two chemically patterned substrates in Ref. [7]. For a single pair of opposing stripes, the wetting phase either forms a bridge spanning from one surface to the other or breaks up into two separate channels. In the case of a plane substrate decorated with many stripes, a whole sequence of morphological transitions has appeared with the number of bridges decreasing as the surface separation between the stripes grows.

Capillary phenomena associated with the presence of a liquid in fibrous bundles are of great importance in a number of fields and products. More recently, fibrous structures have been chosen as scaffold in biology for organism cultivating. To prevent the liquid nutrient from detaching into isolated droplets, the spacing d or the ratio of the spacing d to fiber radius r, has to be maintained to a desirable level.

In the present study, we have extended Princen's approach in several dimensions. First of all we analytically studied the instances $0^\circ \leqslant \theta \leqslant 180^\circ$, or $0 \geqslant S \geqslant -2\gamma$, i.e. to include the cases at the boundaries. For instance, if $\theta = 0^\circ$ and $S = 0$, it is a transition to complete wetting while if $\theta = 180^\circ$ and $S = -2\gamma$, it is a transition to super-hydrophobicity. So we dealt with some wetting cases overlooked in his work, particularly the complete wetting and super-hydrophobic ones. Note that although both θ and $S = \gamma_{SV} - \gamma_{SL} - \gamma$ are used to describe the wetting behavior, the spreading parameter S covers more grounds. For example there are instances where $\theta = 0^\circ$ but $S > 0$, i.e. $\gamma_{SV} - \gamma_{SL} > \gamma$, also termed as complete wetting hereafter, which is common in such materials as iron in contact with mineral oils [8]. Likewise cases where $\theta = 180^\circ$ but $S < -2\gamma$ or $\gamma_{SL} - \gamma_{SV} > \gamma$ indicate a super-hydrophobic repulsive behavior which is explained in detail next.

Consider a complete wetting case so that $S > 0$, i.e. $\gamma_{SV} - \gamma_{SL} > \gamma$. Then image the vapor ($V$) and liquid ($L$) phases exchange the roles so that the vapor is treated as a liquid phase (L) and the liquid as vapor (V). Thus a new spreading parameter $S' = \gamma_{SL} - \gamma_{SV} - \gamma$ is defined (obviously γ is unchanged since $\gamma = \gamma_{LV} = \gamma_{VL}$). Since $S > 0$ or $\gamma_{SV} - \gamma_{SL} > \gamma$, replacing here in terms of S' will result in $S' < -2\gamma$. In other words, this is a reversed super-hydrophobic case where, instead of total spreading of a liquid over a solid in a gaseous environment, we obtain a super-hydrophobic repulsion between a gas bubble submerged into a liquid contacting a solid surface; this should be observable at least in space with absence of any gravity field.

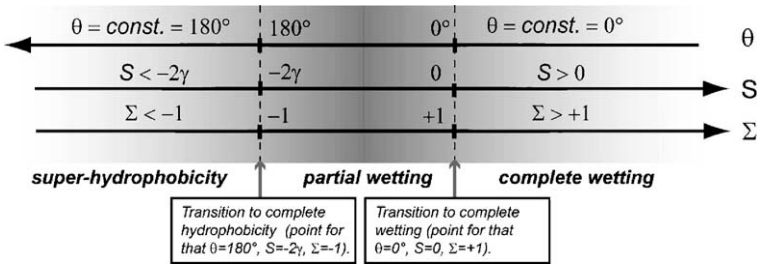

Fig. 1. Three wetting stages (super-hydrophobic, partial wetting, and complete wetting) are divided by two transition points (transition to super-hydrophobicity and transition to complete wetting).

A graphical illustration is depicted in Fig. 1 of the above-described three distinctive wetting cases, i.e., super-hydrophobic, partial wetting, and complete wetting, together with two thresholds between them. That is, a transition to super-hydrophobicity and a transition to complete wetting. These cases and transitions can be described using three parameters θ, S, and $\sum$ the last of which will be defined in Eq. (10) as $\Sigma = \left(S/\gamma + 1\right)$.

We carry out also in this work an analytical derivation of the cross-sectional shapes of the liquid columns between two- and three-cylinder bundles, which will provide us with the complete geometrical information on the relationships among the dimensionless cylinder–cylinder separation d/r, the contact angle θ or the spreading parameter S and another yet to be defined parameter angle α, so as to fully describe the liquid-column shapes.

The lengths of the liquid columns will not play any role in our analysis since the columns are long enough to neglect the effects at the column terminal fronts, where liquid body forms a complex meniscus shape. This is quite consistent with the cases dealt with by Princen in his works [1–3]. Carroll reported in Ref. [9], while studying small liquid drops adhering to a short cylindrical fiber, a different type of transition between axially symmetric and unsymmetric conformations of the droplets.

Next, we conduct a parametric study of the morphological transitions using analytical results obtained, aiming at the construction of morphology diagrams, and we also investigate the hysteresis occurring during the morphological transitions. Finally, we carry out some experimental work to yield results so as to substantiate our analytical predictions.

2. Theory

2.1. Liquid columns between two solid cylinders

Consider a mixture of limited amount of a liquid phase denoted as L with a vapor phase V. The liquid phase L is located within the gap between two narrowly spaced cylindrical solids S. (Our use of the same symbol S for denotation of both the spreading parameter and the solid phase should not cause confusion in the given context.) We will concentrate on wetting structures that are at least of the size of microns so as to ignore both the line tension, and more importantly the gravitational effects. We assume the liquid phase L forms a short bridge whose surface possesses a constant mean curvature $1/R$ (see Fig. 2). When the bridge contains sufficient amount of the phase L, it will then form a long column with constant cross-section.

For convenience, we use the same notations as used by Princen in Ref. [3]. The distance between the solid cylinders is $2d$, and the cylinder diameter is $2r$. Phases L, V and S are characterized by the liquid contact angle θ or by the Harkinson parameter S. The angle between the lines connecting the cylinder centers and the radius to the triplet L–V–S line is noted here as the 'covering angle' α. The radius R represents the curvature of the liquid surface and its value with respect to Laplace pressure is considered positive when the surface is concave, and negative otherwise [1–3]. The cross-section of such a concave long liquid column in the region of constant geometry with positive value of R is shown in Fig. 2.

Princen has treated the equilibrium columns and their surfaces using the principle of minimization of free energy in Ref. [3], whilst we prefer the mechanical concept of surface tension. Adamson and Gast argued in Ref. [8] for the mathematical equivalence of the two concepts.

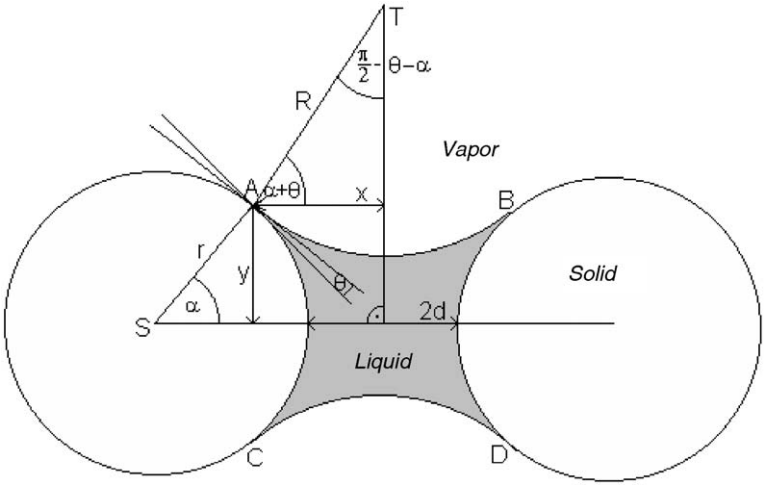

Fig. 2. The cross-section of a pair of parallel cylinders with a long stabile liquid column between them. The cylinder radius is r, the curvature of the free surface of the liquid column is denoted $1/R$, the distance between cylinders is $2d$, and the contact angle is marked by θ. The meaning of the covering angle α is evident from the figure.

To find the cross-sectional shape of the long liquid column at equilibrium between two cylinders we start with a simple case of the column geometry. From the sketch in Fig. 2, we have

$$\frac{R}{r} = \frac{1 + d/r - \cos\alpha}{\cos(\theta + \alpha)}. \tag{1}$$

Our aim however is to find the relationship between the dimensionless inter-cylinder half distance d/r on one side and angles α, and θ or S on the other. Such a relation exists, as we will show later, because R/r depends unambiguously on α and θ (or on spreading parameter S) only. To obtain the relationship we examine the force equilibrium on the liquid column front edge for a concave liquid columns surface depicted in Fig. 2.

$$F_{SV} = F_{LS} + F_{LV} + F_p, \tag{2}$$

where F_{SV} is the force of solid–vapor interface generated by the corresponding surface tension γ_{SV}. This force acts outside the liquid body and tends to spread the liquid along the cylinders. We call F_{SV} the line force because it is proportional to the length of the line, whereas γ_{SV} acting in perpendicular direction to this line and parallel with the cylinder axis. The lines in this case consists of two arcs AC and BD of identical length $L_{AC} = L_{BD} = l_{AC}r$ where $l_{AC} = 2\alpha$. For F_{SV} the following holds:

$$F_{SV} = 2\gamma_{SV} l_{AC} r. \tag{3}$$

Inwards the liquid body along the same arcs acts the force F_{SL} due to the surface tension γ_{LS} between the solid cylinder and the liquid column:

$$F_{LS} = 2\gamma_{LS} l_{AC} r. \tag{4}$$

The last line force F_{LV} is associated with the $L{-}V$ fluid interface. This force acts in the same direction as F_{LS} along the arcs AB and CD, both equal arc lengths L_{AB} and L_{CD}, i.e. $L_{AB} = L_{CD} = l_{AB}R$, where $l_{AB} = 2(\pi/2 - \theta - \alpha)$. So we have for F_{LV}

$$F_{LV} = 2\gamma l_{AB} R \tag{5}$$

Finally F_p, the last quantity in Eq. (2) is the force that has its origin from the Laplace pressure p. The value of Laplace pressure depends on the liquid surface tension γ and the main curvatures $1/R_1$ and $1/R_2$ of the L–V interface via the relation [8]

$$p = \gamma\left(\frac{1}{R_1} + \frac{1}{R_2}\right).$$

In the case of long liquid column between two cylindrical fibers, the L–V interface shares the shape of a portion of the cylinder surface, and hence one of the main curvatures is zero. Thus

$$p = \frac{\gamma}{R} \tag{6}$$

This Laplace pressure acts on the cross-sectional area A of the column, causing the force $F_p = Ap$. Convex liquid surfaces with negative R lead to positive Laplace pressure that tends to spread the liquid along the cylinder while positive radii R of concave liquid surfaces cause liquid suction with the tendency to shrink columns.

The area A can be expressed as seen in Fig. 2, as

$$A = A_{ABCD} - 2A_{AB} - 2A_{AC}, \tag{7}$$

and the areas A_{ABCD}, A_{AB} and A_{AC} satisfy

$$A_{ABCD} = a_{ABCD} rR \quad \text{where } a_{ABCD} = 4\cos(\theta+\alpha)\sin\alpha, \tag{8a}$$

$$A_{AB} = a_{AB}R^2 \quad \textit{where } a_{AB} = \frac{l_{AB}}{2} - \cos(\theta+\alpha)\sin(\theta+\alpha), \tag{8b}$$

$$A_{AC} = a_{AC}r^2 \quad \text{where } a_{AC} = \frac{l_{AC}}{2} - \sin\alpha\cos\alpha. \tag{8c}$$

Substitution of Eq. (3)–(8) together with the relation $F_p = Ap$ into Eq. (2) gives us

$$2\gamma_{SV} l_{AC} r = 2\gamma_{SL} l_{AC} r - 2\gamma l_{AB} R + \left(a_{ABCD} rR - 2a_{AB}R^2 - 2a_{AC}r^2\right)\frac{\gamma}{R}. \tag{9}$$

As opposed to Princen [1–3] as mentioned in the Introduction and in Fig. 1, we will distinguish between several different wetting instances. The first case is the partial wetting scheme with the contact angle $0^\circ < \theta < 180^\circ$, or the spreading coefficient $0 > S > -2\gamma$. Outside this interval lie the realms of complete wetting $\theta = 0^\circ$ and $S > 0$, with a transition point that divides partial wetting from complete wetting case $\theta = 0^\circ$ and $S = 0$. Another is the super-hydrophobic case $\theta = 180^\circ$ and $S < -2\gamma$, and the transition point $\theta = 180^\circ$ and $S = -2\gamma$ that divides the region of partial wetting from the super-hydrophobic area.

Using either the Young equation $\gamma_{SL} - \gamma_{SV} = -\gamma\cos\theta$ or the spreading parameter $S = \gamma_{SV} - \gamma_{SL} - \gamma$ and multiplying Eq. (9) by $R/(r^2 2\gamma)$ yields a quadratic relationship for the dimensionless parameter R/r:

$$a_2\left(\frac{R}{r}\right)^2 + 2b_2\frac{R}{r} + c_2 = 0, \tag{10}$$

where

$$a_2 = l_{AB} - a_{AB} = \left(\frac{\pi}{2} - \theta - \alpha\right) + \sin(\theta+\alpha)\cos(\theta+\alpha), \tag{10a}$$

$$\begin{aligned} b_2 &= \left(\tfrac{1}{2}a_{ABCD} - l_{AC}\cos\theta\right) = \sin\alpha\cos(\theta+\alpha) - \alpha\cos\theta \\ &= \sin\alpha\cos(\theta+\alpha) - \alpha\Sigma, \end{aligned} \tag{10b}$$

and $\sum = \left(S/\gamma + 1\right)$.

So for complete wetting (CW), i.e. $\theta = 0^\circ$, Eq. (10b) becomes

$$b_{2,CW} = \sin\alpha\cos\alpha - \alpha\Sigma = c_2 + \alpha(1-\Sigma). \tag{10bCW}$$

and for the super-hydrophobicity (SH), $\theta = 180^\circ$

$$b_{2,SH} = -\sin\alpha\cos\alpha - \alpha\Sigma = -c_2 - \alpha(1+\Sigma), \tag{10bSH}$$

where

$$c_2 = -a_{AC} = \sin\alpha\cos\alpha - \alpha, \tag{10c}$$

is universal for all wetting situations. By using the symbol $\sum$ and c_2, parameters $b_{2,CW}$ and $b_{2,SH}$ can thus be expressed in more general forms.

The solution of the quadratic Eq. (10) is

$$\left(\frac{R}{r}\right)_{1,2} = \frac{-b_2 \pm \sqrt{b_2^2 - a_2 c_2}}{a_2}, \tag{11}$$

depending on α and θ only as evidenced from the definitions of the parameters a_2, b_2, and c_2.

After substituting Eq. (11) into Eq. (1), we derive the relation between d/r and the angles α and θ:

$$\left(\frac{d}{r}\right)_{1,2} = \left(\frac{-b_2 \pm \sqrt{b_2^2 - a_2 c_2}}{a_2}\right) \cos(\theta + \alpha) + \cos\alpha - 1. \tag{12}$$

For partial wetting cases, the physically acceptable solution is the one with positive square root that ensures the positive value of d/r.

For the particular case of transition to complete wetting when $S = 0$, $\sum = 1$ and $\theta = 0^\circ$, we have $a_2 = c_2 + \pi/2$ and $b_2 = c_2$ so that

$$\left(\frac{d}{r}\right)_{S=0} = \left(\frac{-c_2 + \sqrt{-\frac{\pi c_2}{2}}}{\frac{\pi}{2} + c_2}\right) \cos\alpha + \cos\alpha - 1. \tag{13}$$

To include the complete wetting case $S \geqslant 0$ and $\theta = 0^\circ$, the wetting phenomenon is then governed by parameters $\alpha_{2,CW} = c_2 + \pi/2$ and $b_{2,CW} = c_2 - \alpha(1 - \sum)$. Then Eq. (12) reduces to

$$\left(\frac{d}{r}\right)_{CW} = \left(\frac{\alpha(\Sigma - 1) - c_2 + \sqrt{\alpha(\Sigma - 1)[\alpha(\Sigma - 1) - 2c_2] - \frac{\pi c_2}{2}}}{\frac{\pi}{2} + c_2}\right) \cos\alpha + \cos\alpha - 1. \tag{13CW}$$

When the liquid is completely repelled by cylinders, i.e. $S \geqslant -2\gamma$ and $\theta = 180^\circ$ so that $\alpha_{2,SH} = c_2 - \pi/2$, and $b_{2,SH} = -c_2 - \alpha(1 - \sum)$, only the solution of Equation (12) with the negative sign with the square root provides us with positive $(d/r)_{SH}$ values.

$$\left(\frac{d}{r}\right)_{SH} = \left(\frac{c_2 + \alpha(\Sigma + 1) - \sqrt{\alpha(\Sigma + 1)[2c_2 + \alpha(\Sigma + 1)] + \frac{\pi c_2}{2}}}{c_2 - \pi}\right) \cos\alpha + \cos\alpha - 1. \tag{13SH}$$

In Fig. 3 we have plotted d/r according to Eqs. (13), (13CW) and (13SH). Princen indicated in Ref. [3] that only the increasing parts of the d/r versus α curves in Fig. 3a are stable solutions and the rest solutions are at equilibrium but unstable, for a decreasing d/r value indicates leaking or disintegration of the liquid column.

Fig. 3a illustrates d/r versus the covering angle α for partial wetting case, where a larger α value, i.e. a wider covering arc AC of the liquid meniscus, or a smaller contact angle θ, leads to a greater d/r value, i.e. more volumetric liquid contained. Fig. 3b depicted the complete wetting situation $\theta = 0^\circ$, where in general much more water (much greater d/r) is absorbed than in the case of partial wetting; increasing either α or $\sum$ can achieve even greater liquid adsorption.

Finally Fig. 3c shows $d/r \sim \alpha$ dependences for $\sum < -1$, concerning the super-hydrophobic case. All liquid columns, one of them is shown in Fig. 3d, where we can deduce that, any combination of α and $\sum$ which lead to $d/r > 0$ will be unstable. The capillary pressure difference will accelerate the movement of the liquid column boundaries resulting in the leakage of the liquid away from the space in-between a pair of fibers. The escaped liquid body without the support of cylinders will be immediately disintegrated into droplets like a free liquid jet.

Back to the partial-wetting regime, the ultimate covering angle α_{max} yielding $(d/r)_{max}$ at different values of the contact angle θ for stable equilibrium liquid columns are plotted in Fig. 4, whereas the maximum ratio $(d/r)_{max}$ against θ are depicted in Fig. 5a. Numerical results are indicated along the curves hereafter for easy examination.

For the complete wetting case where $\theta = 0^\circ$ and $S > 0$ (i.e. $\sum > 1$) leading to $\alpha = 180^\circ$, we derived directly from (13CW) the simple formula $(d/r)_{max,CW} = 2(\Sigma - 1) + \sqrt{4\Sigma - 2}$ based on which Fig. 5b was plotted. So in this case $(d/r)_{max}$ is simply close to a linear function of the parameter $\sum$.

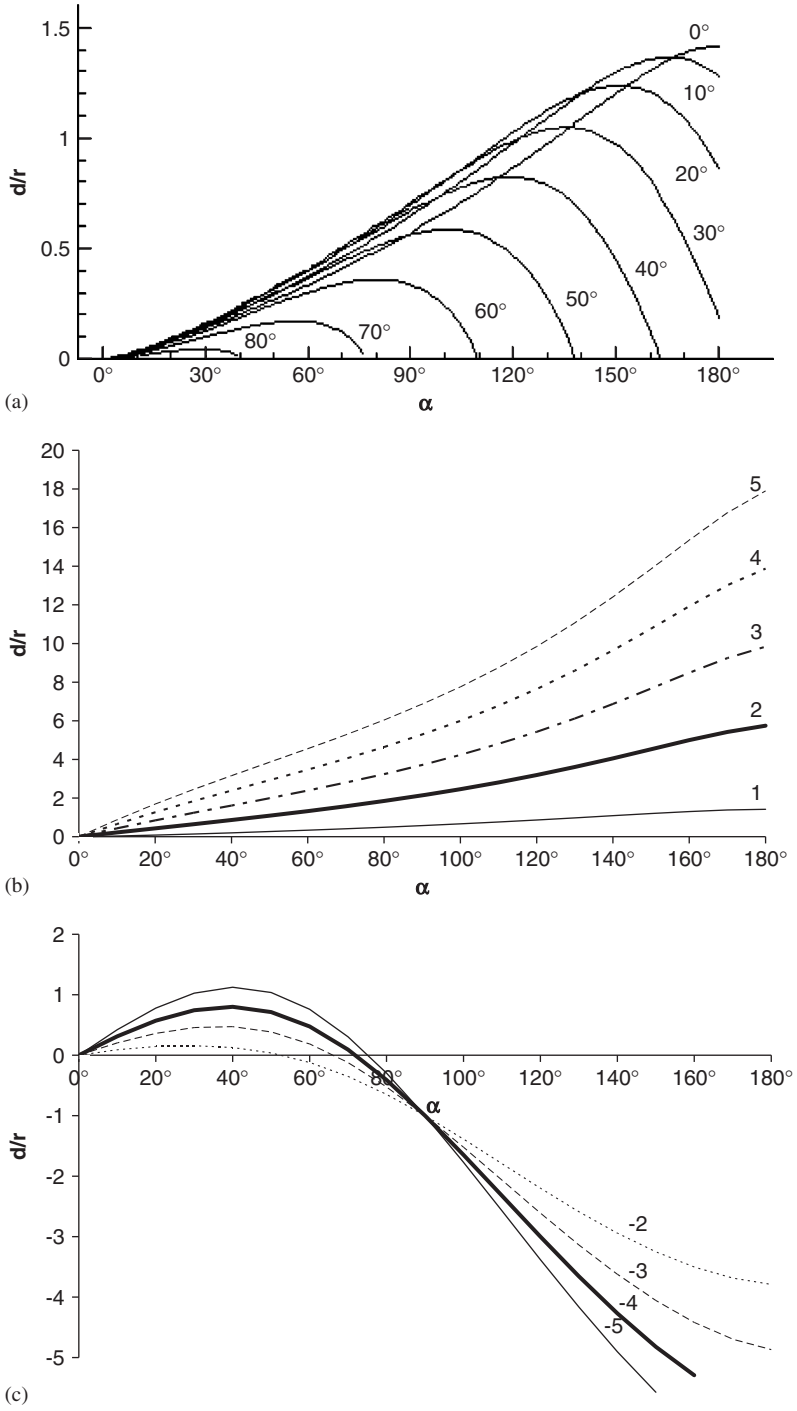

Fig. 3. (a) Relationship between d/r and α for long columns of constant cross-section between two cylinders at nine contact angles θ. These plots cover systems with partial wetting where $\theta \in (0^\circ, 180^\circ)$. (b) Plots of d/r dependence on α for various values $\sum = S/\gamma + 1$ were calculated using Eq. (13CW) for complete wetting regime. The particular $\sum$ values are typed tight to each of corresponding curves. (c) The graphs for super-hydrophobic surfaces express $d/r-\alpha$ dependences calculated according to the Eq. (13SH) for some chosen values $\sum$ below–1. Nonzero d/r values were obtained using the minus sign in front of the second root of solution (12). (d) A cross-section of unstable long liquid columns for super-hydrophobic pairs of cylinders. Each perturbation of cylindrical liquid boundaries will lead to its inexorable going-on thanks to a decrease of the capillary pressure on the head liquid front and its increase on the back. The movement of such perturbation is envisaged by arrows.

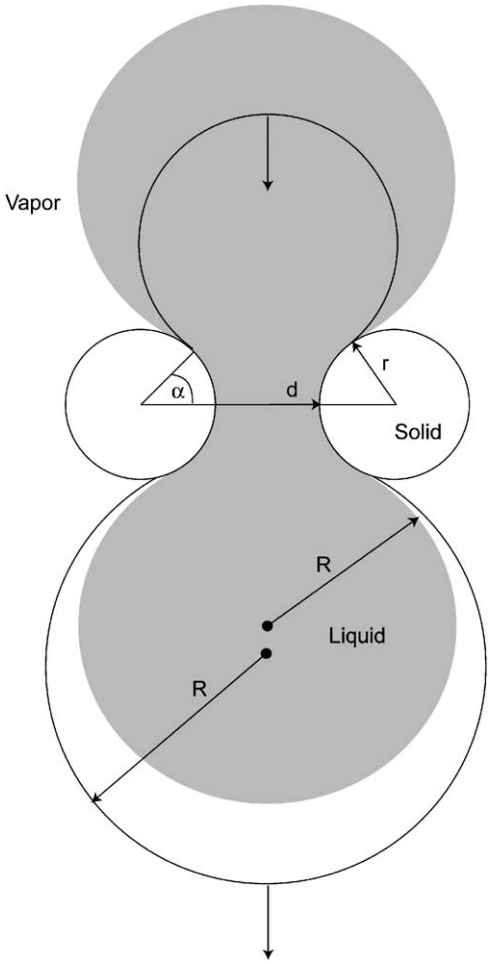

Fig. 3. (*Continued*)

Fig. 6 shows some cross-sectional shapes of the liquid column between the two cylinders for $\theta = 0^\circ$ and $\theta = 40^\circ$, respectively. The figures were plotted using Eq. (12).

We will use the above results in next section to describe the morphological transitions of the liquid columns between two cylinders and three separate columns with channel-filling liquid column.

2.2. Liquid columns among three solid cylinders

A typical cross-section of a channel-filing liquid column among three equal-distance and horizontal cylinders is shown in Fig. 7. The notations in the figure are similar to those used above for two-cylinder system, except for the definition for angle α.

The angle α is now the one between the line connecting the centers of neighboring cylinders and the radius to the L–V–S boundary. It means that the meaningful upper limit of α for non overlapping liquid surfaces is now 150°, and in three-cylinder case 2α no longer covers the entire wetted region for each cylinder, although for convenience it is still called the covering angle. To distinguish the two- and three-cylinder systems, we will use both a stroke for three-cylinder quantities and the index 3 for parameters a, b, c in the following text.

The equilibrium condition for channel-filing liquid column is the same as for that in two-cylinder system, as expressed by Eq. (2). The force F'_{SV}, driving the liquid to spread along cylinders, is composed now by three

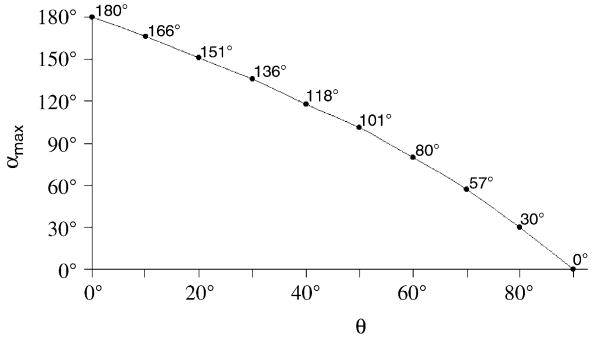

Fig. 4. The relationship between the maximal values of the covering angle α and the contact angle θ for two-cylinder bundle. Numerical values of α_{max} for chosen contact angles $\theta = \{0^0, 10^0, 20^0, 30^0, 40^0, 50^0, 60^0, 70^0, 80^0, 90^0\}$ are introduced directly in the graph.

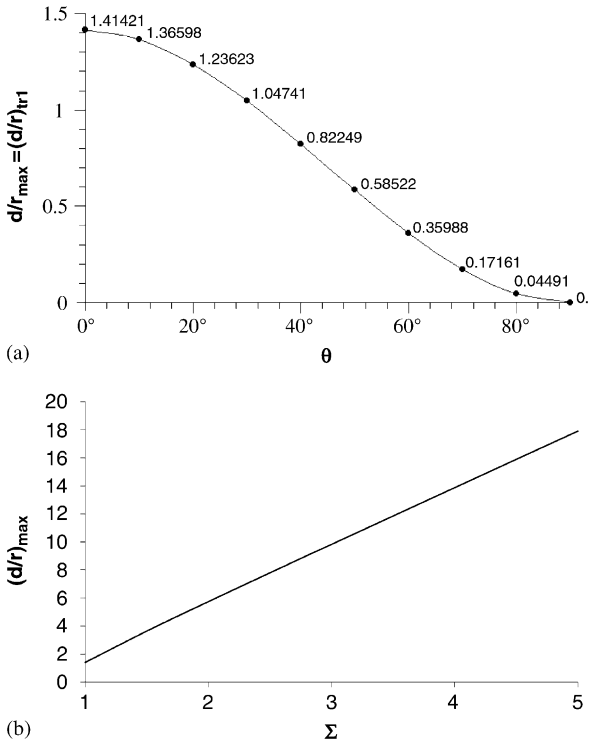

Fig. 5. (a) The dependence of the maximal values of d/r on the contact angle θ. Numerical values of $(d/r)_{max}$ for chosen contact angles $\theta = \{0^0, 10^0, 20^0, 30^0, 40^0, 50^0, 60^0, 70^0, 80^0, 90^0\}$ are shown in the figure. (b) Relationship $\left(d/r\right)_{\max,CW} = 2(\Sigma - 1)\sqrt{4\Sigma - 2}$ for maximal d/r values in the case of completely wetting pair of cylindrical fibers.

arcs of equal length $L'_{AC} = \left(l_{AC} + \pi/3\right)r$, where $l_{AC} = 2\alpha$ is the same as in the two-cylinder case. Hence for F'_{SV} due to the surface tension between the solid and the vapor we have

$$F'_{SV} = (3l_{AC} + \pi)r\gamma_{SV}. \tag{14}$$

Another force F'_{SL} acts along the same three arcs as F'_{SV}, but in opposite direction. It is due to the surface tension γ_{SL} acting on the solid–liquid interface.

$$F'_{SL} = (3l_{AC} + \pi)r\gamma_{SL}. \tag{15}$$

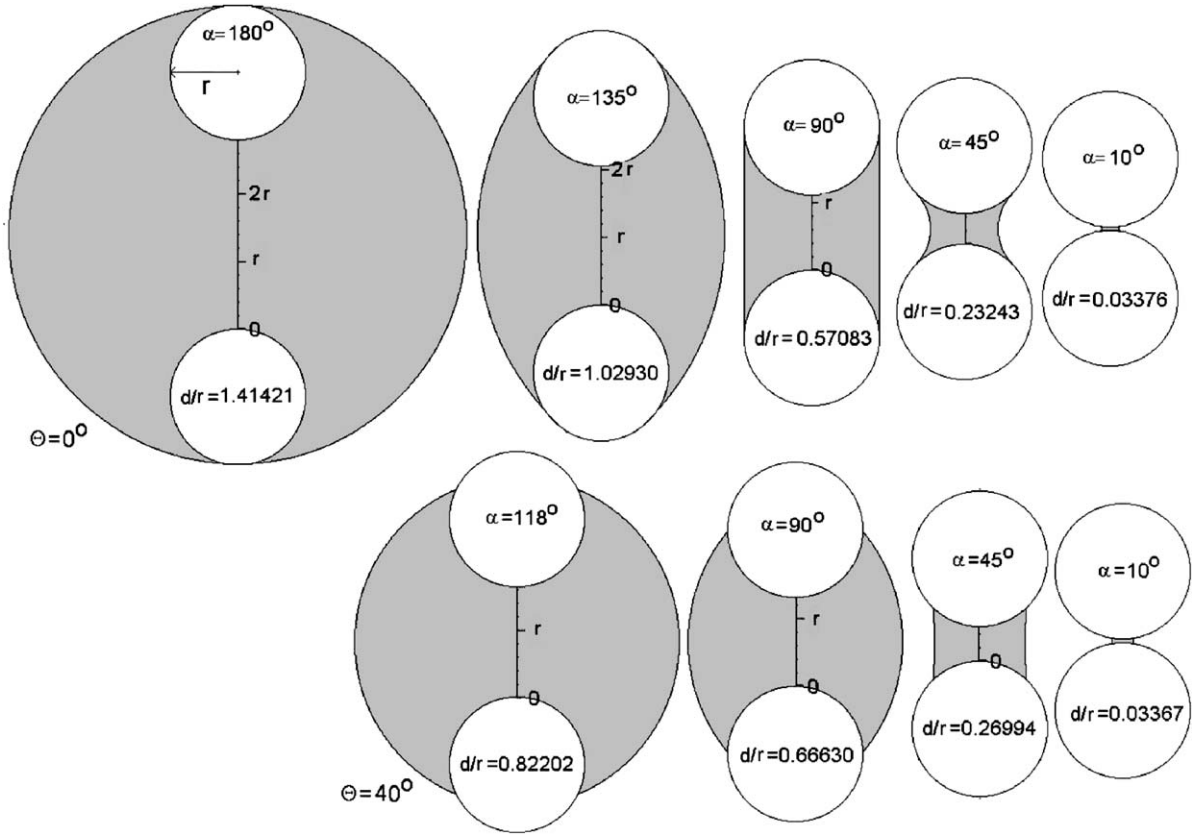

Fig. 6. Several cross-sectional shapes of liquid columns in two-cylinder system for $\theta = 0°$, and $\theta = 40°$. The first cross-sections from the left of each series represent the states with maximal values of d/r and α. The next increase of the cylinder–cylinder separation will cause abrupt change of the liquid-body shape. The long column will change into an ''unduloid''.

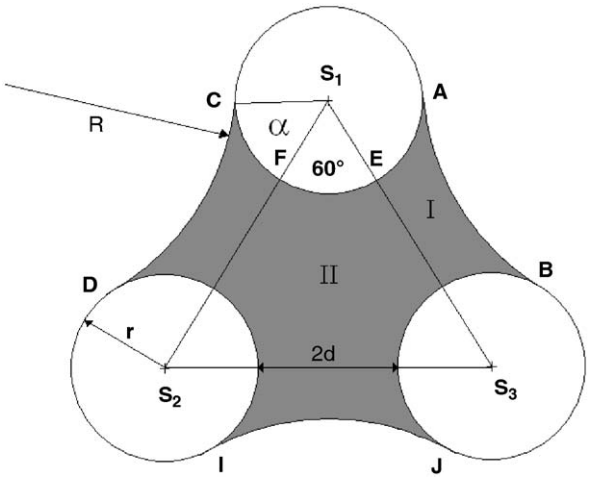

Fig. 7. The cross-section of the three-cylinder system with a channel-filling column among them. The area A of the liquid column cross-section consists of three parts (I), and the component (II).

The last line force F'_{LV} in the equilibrium equation is the one associated with the surface tension γ between the liquid and its vapor. It acts along three arcs of length $L_{AB} = l_{AB}R$, which are expressed in the same manner as in the two-cylinder assembly. Hence F'_{LV} satisfies

$$F'_{LV} = 3l_{AB}R\gamma. \tag{16}$$

Note that $l_{AB} = 2(\pi/2-\theta-\alpha)$.

The Laplace pressure force F'_p is the product of the Laplace pressure γ/R with the liquid column cross-sectional area A':

$$F'_p = A'\frac{\gamma}{R}. \tag{17}$$

The area A' can be expressed using two sub-regions denoted as (I) and (II) in Fig. 7. The sub-region (I) has the area $A_I = A/2$, where A is still the same as in Eqs. (7) and (8) for two-cylinder system. Combining these equations yields

$$A_I = \frac{1}{2}a_{ABCD}rR - a_{AB}R^2 - a_{AC}r^2. \tag{18}$$

The sub-region (II) has the area A_{II} derivable from the area of the triangle A_{S1S2S3} that has its summits in the centers of cylinder cross-sections S_1,S_2 and S_3. To obtain A_{II} we have to subtract from the triangle area A_{S1S2S3} three areas of A_{ES_1F} of the circular sector ES_1F. For A_{S1S2S3} it is apparent that

$$A_{S_1S_2S_3} = \sqrt{3}(d+r)^2 = \sqrt{3}[R\cos(\theta+\alpha) + r\cos\alpha]^20 \tag{19}$$

where we have used Eq. (1) to express $d+r$ in terms of R,θ,α and r.

The circular section ES_1F has an area

$$A_{ES_1F} = \pi r^2/6. \tag{20}$$

Hence we have for the cross-sectional area of the liquid column among three cylinders

$$\begin{aligned} A' &= 3A_I + A_{II} = 3A_I + A_{S_1S_2S_3} - 3A_{ES_1F} \\ &= \frac{3}{2}\mathrm{a}_{ABCD}rR - 3\mathrm{a}_{AB}R^2 - 3\mathrm{a}_{AB}r^2 + \sqrt{3}[R\cos(\theta+\alpha) + r\cos\alpha]^2 - \frac{\pi r^2}{2}. \end{aligned} \tag{21}$$

Substituting Eqs. (14)–(17), and (21) into (2) and using the Young equation $\gamma_{SL}-\gamma_S = \gamma\cos\theta$, we obtain the final quadratic equation:

$$a_3\left(\frac{R}{r}\right)'^2 + 2b_3\left(\frac{R}{r}\right)' + c_3 = 0, \tag{22}$$

where

$$a_3 = 3\left(\frac{\pi}{2} - \theta - \alpha\right) + 3\sin(\theta+\alpha)\cos(\theta+\alpha) + \sqrt{3}\cos^2(\theta+\alpha), \tag{22a}$$

$$b_3 = 3\cos(\theta+\alpha)\sin\alpha + \sqrt{3}\cos(\theta+\alpha)\cos\alpha - 3\alpha\cos\theta - \frac{\pi}{2}\cos\theta, \tag{22b}$$

where for complete wetting cases $\theta = 0^\circ$ and for super-hydrophobic ones $\theta = 180^\circ$.

Similar to the manipulations in the 2-cylinder cases, by connecting $\cos\theta$ with the parameter $\sum$, we derive $b_{3,CW}$ for the complete wetting ($S>0$, $\sum>1$, and $\theta = 0^\circ$) as

$$b_{3,CW} = 3\cos\alpha\sin\alpha + \sqrt{3}\cos^2\alpha - \left(3\alpha+\frac{\pi}{2}\right)\sum = c_3 - \left(3\alpha+\frac{\pi}{2}\right)\left(\sum -1\right). \tag{22bCW}$$

For the super-hydrophobic cases, $S\leqslant -2\gamma$ and $\theta = 180^\circ$ the following it holds:

$$b_{3,SH} = -3\cos\alpha\sin\alpha - \sqrt{3}\cos^2\alpha - \left(3\alpha+\frac{\pi}{2}\right)\sum = -c_3 - \left(3\alpha+\frac{\pi}{2}\right)\left(\sum +1\right). \tag{22bSH}$$

The last parameter c_3 is, similar to c_2 universal for all wetting situations.

$$c_3 = \sqrt{3}\cos^2\alpha - \frac{\pi}{2} + 3\sin\alpha\cos\alpha - 3\alpha. \tag{22c}$$

Likewise, the solutions of the quadratic Eq. (22) has two roots:

$$\left(\frac{R}{r}\right)'_{1,2} = \frac{-b_3 \pm \sqrt{b_3^2 - a_3 c_3}}{a_3}. \tag{23}$$

Again combining Eq. (23) with Eq. (1) gives

$$\left(\frac{d}{r}\right)'_{1,2} = \left(\frac{-b_3 \pm \sqrt{b_3^2 - a_3 c_3}}{a_3}\right)\cos(\theta+\alpha) + \cos\alpha - 1. \tag{24}$$

For the case with zero spreading coefficient, i.e., for the transition to complete wetting, ($S = 0$ and $\theta = 0^\circ$), Equation (24) reduces, due to relations $a_3 = c_3 + 2\pi$ and $b_3 = c_3$ following from Eqs. (22a) and (22b), into

$$\left(\frac{d}{r}\right)'_{s=0} = \left(\frac{-c_3 + \sqrt{-2\pi c_3}}{2\pi + c_3}\right)\cos\alpha + \cos\alpha - 1. \tag{25a}$$

For the complete wetting case, $S \geqslant 0$ and $\theta = 0^\circ$,

$$\left(\frac{d}{r}\right)'_{CW} = \left(\frac{\left(3\alpha+\frac{\pi}{2}\right)(\Sigma-1) - c_3 + \sqrt{\left(3\alpha+\frac{\pi}{2}\right)(\Sigma-1)\left[\left(3\alpha+\frac{\pi}{2}\right)(\Sigma-1) - 2c_3\right] - 2\pi c_3}}{2\pi + c_3}\right)\cos\alpha + \cos\alpha - 1, \tag{25CW}$$

since $a_3 = c_3 + 2\pi$ and $b_3 = c_3 - (3\alpha + \pi/2)$ ($\sum - 1$) for $S \geq 0$ and $\theta = 0^\circ$. For super-hydrophobic surfaces, it is given by

$$\left(\frac{d}{r}\right)'_{SH} = \left(\frac{c_3 + \frac{\pi}{2} + \left(3\alpha+\frac{\pi}{2}\right)(\Sigma+1) - \sqrt{\left[c_3 + \frac{\pi}{2} + \left(3\alpha+\frac{\pi}{2}\right)(\Sigma+1)\right]^2 - (c_3 - \pi)c_3}}{c_3 - \pi}\right)\cos\alpha + \cos\alpha - 1. \tag{25SH}$$

The liquid body can be perfectly cylindrical when $\alpha = 150^\circ$, $S \geq 0$ and $\theta = 0^\circ$ as will be shown below while deriving Eqs. (28).

The relationships between $(d/r)'$ and the covering angle α are illustrated for various levels of both the contact angle θ and the parameter $\sum$ in Fig. 8. Once more, the physically stable equilibrium states include only the increasing parts of the curves.

It is noticeable that for three cylinders the equilibrium dimensionless distance $(d/r)'$ reaches its maximum value as $\theta = 20^\circ$ (in Fig. 8a), not $\theta = 0^\circ$ as in the two-cylinder case. The behavior of systems for complete wetting is depicted in Fig. 8b, and for super-hydrophobic surfaces in Fig. 8c, where for positive d/r values the negative sign in Eq. (24) has to be taken. Stable liquid columns are those with $\alpha < 0^\circ$ Fig. 8d depicts cross-sectional shapes of stable and unstable liquid bodies for a super-hydrophobic situation. Similar comments on the stable ranges for θ and $\sum$ can be made as in 2-cylinder cases.

Also for three-cylinder system the liquid absorbed is usually higher than that for the system of two cylinders, as visible from comparison of Fig. 6 with Fig. 9, where the cross-sectional shapes of liquid bodies are illustrated for the two systems, respectively, at chosen levels of θ.

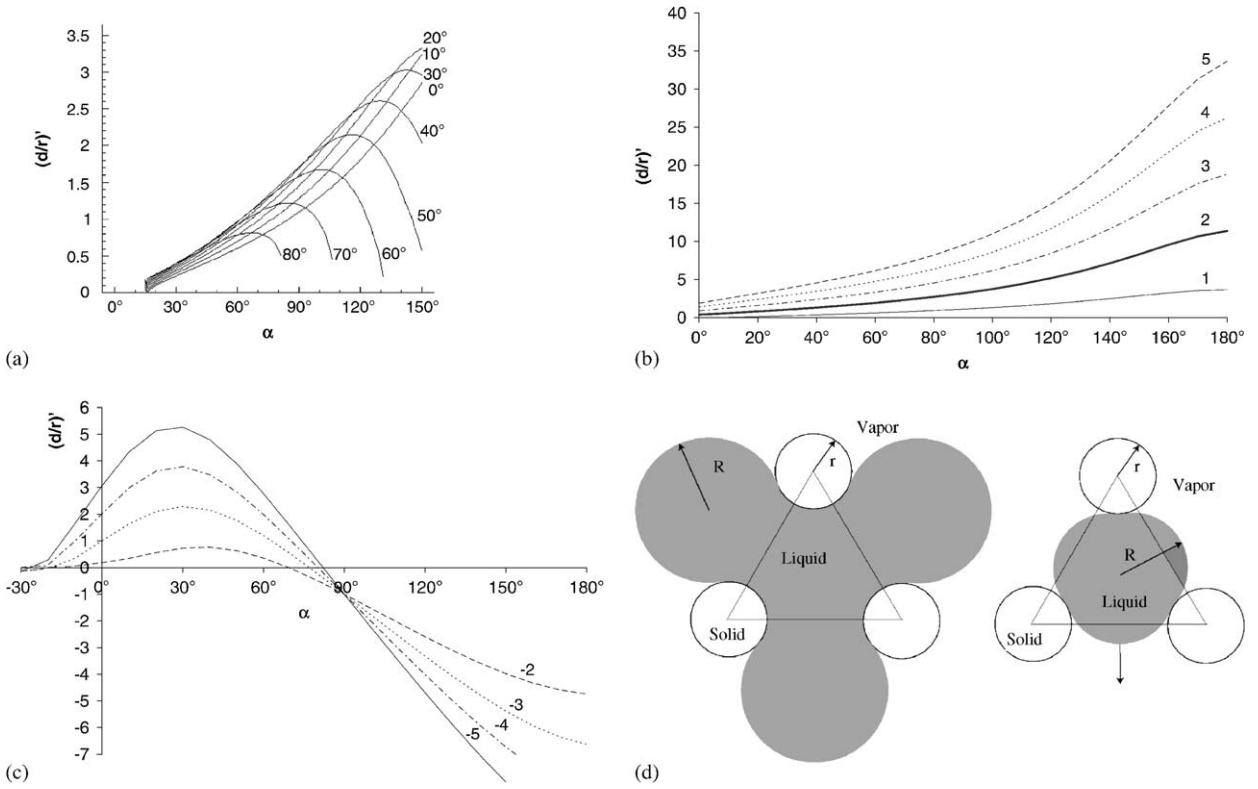

Fig. 8. (a) The graphs show the dependence of the dimensionless cylinder–cylinder separation $(d/r)'$ on the covering angles θ for various contact angles θ for three-cylinder bundles. (b) The dependences of $(d/r)'$ on α for complete wetting instances are depicted for chosen values $\sum = \{1, 2, 3, 4, 5\}$. (c) Dependences of the dimensionless parameter $(d/r)'$ on α for super-hydrophobic cylinder surfaces. Individual curves belong to five chosen values $\sum = \{-1, -2, -3, -4, -5\}$. (d) Drawings of cross-sections of an unstable (left-hand side) and a stable (right-hand side) long liquid columns for high values of contact angle $\theta \approx 180^o$ or for super-hydrophobic surfaces, i.e. $S < -2\gamma$, $\sum < -1$.

3. Morphological transitions

3.1. Liquid body morphological transition in two-cylinder systems

When the cylinder–cylinder separation between two cylinders becomes greater than a certain threshold value $(d/r)_{tr}$, the liquid column between the two cylinders can no longer maintain a single cross-section and will instead turn into a shape similar to a sessile droplet, or unduloid, on a single fiber. The threshold or transition value $(d/r)_{tr}$ depends on among other things the values of α or θ or S. It is in fact obvious that $(d/r)_{tr} = (d/r)_{max}$.

The covering angle leading to $(d/r)_{tr}$ is α_{max} which is related to the contact angle θ as shown in Fig. 4. The special case of the transition to complete wetting $S = 0$ is provided by Eq. (13) for $\alpha = \alpha_{max} = 180^\circ$ and $c_2 = -\pi$. Hence the value $(d/r)_{max,S=0} = \sqrt{2} = 1.41421$ is the upper limit to which the liquid column can still reverse back to the original stable state.

For spreading parameter values greater than zero, i.e. for the complete wetting case, inter-cylinder distance obeys the formula $(d/r)_{max,CW} = 2(\Sigma - 1) + \sqrt{4\Sigma - 2}$ that has been derived in the Section 2.1. The relative water absorbed d/r has evidently no theoretical limit for its growth with increasing S as seen in Fig. 5b.

Conversely, on starting with a ratio $d/r > (d/r)_{tr}$ and drawing the cylinders closer, we suppose the threshold shape of a limited amount of liquid will be a long cylinder encircling the two cylinders as shown in Fig. 10. There is then a simple expression for the area A of the cross-section as the area of a circle with the radius R from which we subtract two circle areas each of the radius r. The Laplace force F_p is now $-\pi(R^2 - 2r^2)\gamma/R$ and

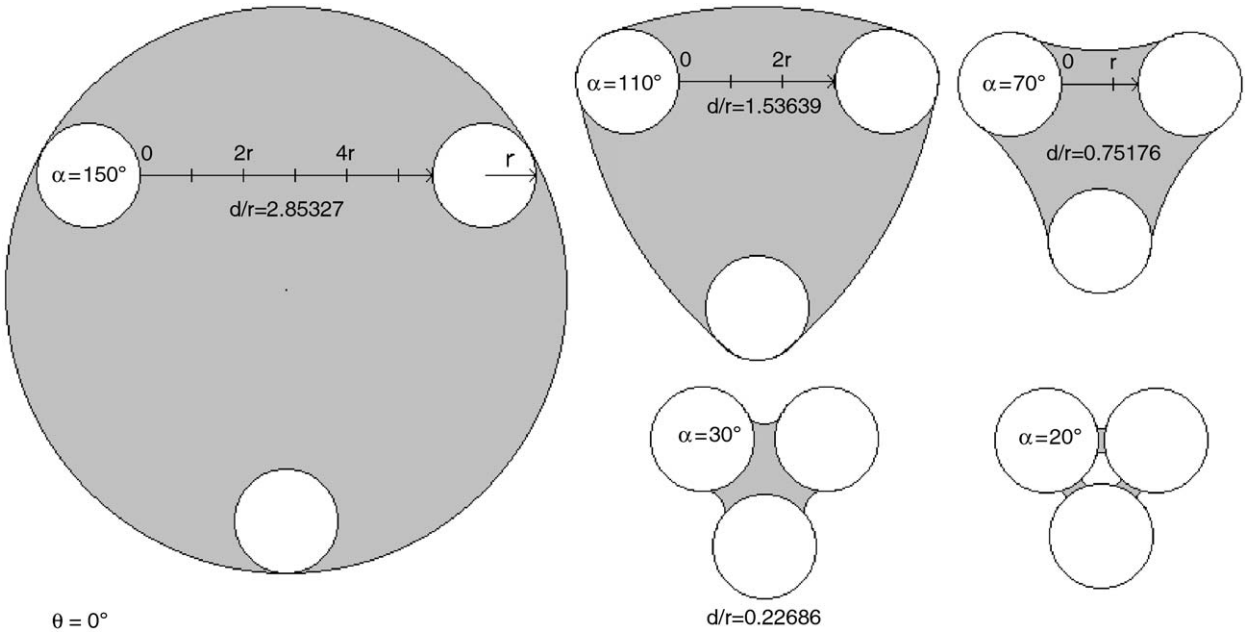

Fig. 9. Several cross-sectional shapes of liquid columns in three-cylinder system for $\theta = 0^\circ$. The first cross-section from the left represents the state with maximal value of d/r and α. Next increase of the cylinder–cylinder separation will cause the abrupt change of the liquid body shape. The long column will turn into the "unduloid".

the Eq. (2) reduces to

$$4\pi r\gamma_{SV} = 4\pi r\gamma_{LS} + 2\pi R\gamma - \pi\left(R^2 - 2r^2\right)\frac{\gamma}{R}, \tag{26}$$

where a negative R has been used due to the convex shape of the cylindrical liquid body. Relation (26) provides us with the quadratic equation (27)

$$\left(\frac{R}{r}\right)'^2 + 4\cos\theta\left(\frac{R}{r}\right)'^2 + 2 = 0 \tag{27}$$

with the solutions $\left(R\Big/r\right)'_{1,2} = -2\cos\theta \pm \sqrt{2}\sqrt{2\cos^2\theta - 1}$. A physical sense requires $|R| \geqslant 2r$, i.e., the negative sign before the second term be taken. The covering angle α is 180° as illustrated in Fig. 10 so that holds– $R = 2r + d$. Substituting this relation into Eq. (27) we obtain the relationship between $(d/r)'_{tr2}$ and θ. For partial wetting region with θ ranges over (0°, 180°)

$$\left(\frac{d}{r}\right)'_{tr2} = 2(\cos\theta - 1) + \sqrt{4\cos^2\theta - 2}. \tag{28}$$

The case of complete wetting ($S > 0$, i.e. $\sum > 1$) is governed by the following relationship:

$$\left(\frac{d}{r}\right)_{tr2,CW} = 2(\Sigma - 1) + \sqrt{4\Sigma^2 - 2}. \tag{28CW}$$

The special transition for $S = 0$ ($\theta = 0^\circ$) occurs when $\left(d/r\right)'_{tr2} = 2(1-1) + \sqrt{2} = \sqrt{2}$ as derived directly from both Eqs. (28) and (28CW). This result is identical to the above transition value $(d/r)_{tr1}$ from Eq. (13).

The hysteresis of the transitions for partial wetting area emerges as the result of the difference between the values $(d/r)_{tr1}$ calculated directly from Eq. (12) and the threshold values $(d/r)_{tr2}$ from Eq. (28). Both transition curves are plotted in Fig. 11 to evaluate the difference between them.

Assume one starts with a cylinder–cylinder separation greater than the threshold value $2(d/r)_{tr1}$ with the liquid originally forming an unduloid. While the distance between cylinders decreases, the unduloid

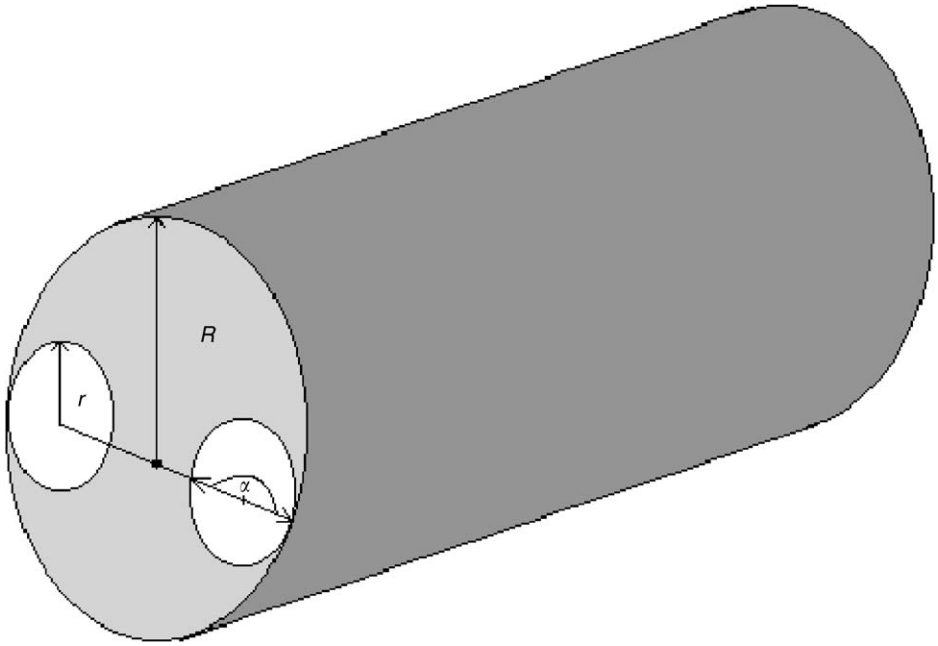

Fig. 10. System composed of two cylinders with long liquid column of the cylindrical shape. The cylinders are touching the liquid body from the inside. The situation on the figure belongs to the threshold $(d/r)_{tr2}$.

gradually prolongs until it suddenly turns into a cylindrical liquid body upon touching the two solid cylinders in one point. This transition is governed by Eq. (28). Moving the two cylinders even closer to each other, the dry areas on each cylinder will appear. Then if the cylinders are slowly separated again to complete the hysteresis loop, the previously dry cylinder surfaces are now coated by a liquid film so that Eq. (12) becomes effective. These different transition conditions during the reversal in fact are the causes for the hysteresis.

3.2. Transition from multiple columns to channel-filling column in three cylinder system

Princen in his work [3] made an assumption that at small cylinder–cylinder distance $2d$, the liquid column in between the three cylinders disintegrates into three separate columns, one between each pair of the adjacent cylinders. Thus, a hole forms all along the center of the disappeared column. Princen has offered two alternative justifications. The first is based on the comparison of surface free energies of the channel-filling and disintegration morphologies of columns. The second one is by considering liquid flows in the case of coexistence of both morphologies in the same system; the coexistence will cause the liquid flow from higher pressure regions to the lower ones. The result of the flow is the extinction of the higher pressure column shape.

The pressure difference is governed by the Laplace pressure formulas. That is why the transition between separate columns and channel-filling column occurs under the condition of equal values of curvatures $1/R$ of the liquid bodies. The numerical solution for a general contact angle θ in the case of partial wetting is obtained by equating Eq. (11) to Eq. (23), i.e.,

$$\frac{-b_2+\sqrt{b_2^2-a_2c_2}}{a_2}=\frac{-b_3+\sqrt{b_3^2-a_3c_3}}{a_3}. \tag{29}$$

The resultant transition curve based on this relation is sketched as the curve no.1 in the morphology diagram in Fig. 12.

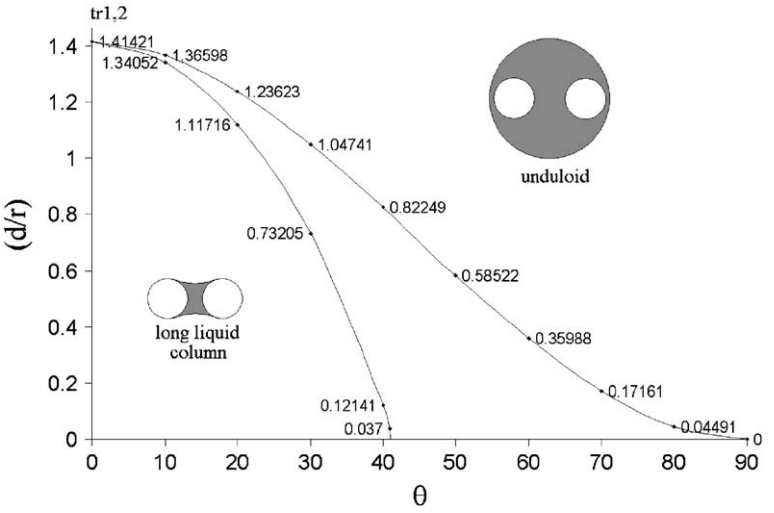

Fig. 11. The morphology diagram for transitions between long liquid columns and "unduloids" for two parallel cylinders under the conditions of partial wetting. The d/r–θ relationship curve (1) depicts transitions from long liquid columns to "unduloids" and is identical with the one shown in Fig. 5, while curve (2) describes morphological changes from a perfectly cylindrical liquid-body shape to a long liquid column.

When $S = 0$ ($\theta = 0^\circ$), i.e. at the complete wetting threshold, Eq. (29) turns into

$$\frac{-c_2 + \sqrt{-\frac{\pi c_2}{2}}}{\frac{\pi}{2} + c_2} = \frac{-c_3 + \sqrt{-2\pi c_3}}{2\pi + c_3}. \tag{30}$$

After the substitution $c_3 = 4c_3'$ we can rewrite Eq. (30) into

$$\frac{-c_2 + \sqrt{-\frac{\pi c_2}{2}}}{\frac{\pi}{2} + c_2} = \frac{-c_3' + \sqrt{-\frac{\pi c_3'}{2}}}{\frac{\pi}{2} + c_3'}. \tag{31}$$

According to Eqs. (10c) and (22c), values of c_2 and c_3' are both negative for α from intervals $\alpha \in (0, \pi)$ and $\alpha \in (0.25, 5\pi/6)$, respectively. These c's values are then fall into corresponding intervals $c_2 \in (0, -\pi)$ and $c_3' \in (0, -3\pi)$. On the joint interval $c_2, c_3' \in (0, -\pi)$ are both functions given by the terms on RHS and LHS of Eq. (31) positive and monotonically decreasing.

So Eq. (31) is true only if $c_2 = c_3'$. Thus, the threshold condition for $S = 0$ is reached. The threshold value α'_{tr1} for zero contact angle θ and zero spreading parameter S, i.e. on the threshold to complete wetting, is therefore given by

$$\sqrt{3}\cos^2 \alpha'_{tr1} - \sin \alpha'_{tr1} \cos \alpha'_{tr1} + \alpha'_{tr1} = \frac{\pi}{2}. \tag{32}$$

The numerical solution shows $= \alpha'_{tr1} = 0.333305\,\text{rad} = 1/3\,\text{rad}$ or $(d/r)'_{tr1} = 0.07869$. The complete wetting region with S>0 and $\sum > 1$ leads to more complicated relation that has to be solved numerically, since Eqs. (13CW) and (25CW) that contain the information about R/r, have to be used in their general forms.

Morphological transition between the channel-filling liquid column and the separate liquid columns also has a hysteresis as noted in Ref. [3], confirmed by the above-derived threshold values. Assume one starts with a cylinder–cylinder separation greater than the threshold value $2(d/r)'_{tr1}$ with the liquid column originally filing the channel. When the distance is decreased a hole will form and the channel-filling liquid column starts to split (when $\theta = 0^\circ$ and $S = 0$ this transition occurs for $(d/r)'_{tr1} = 0.07869$ as mentioned before). If the cylinders are subsequently separated again, i.e., the distance is increased to complete the hysteresis loop, previously split liquid columns survive until α increases to 30° when the separated liquid columns connect each other again at $(d/r)_{tr2}$, and the central hole disappears. These different transition conditions in fact are the cause for the hysteresis.

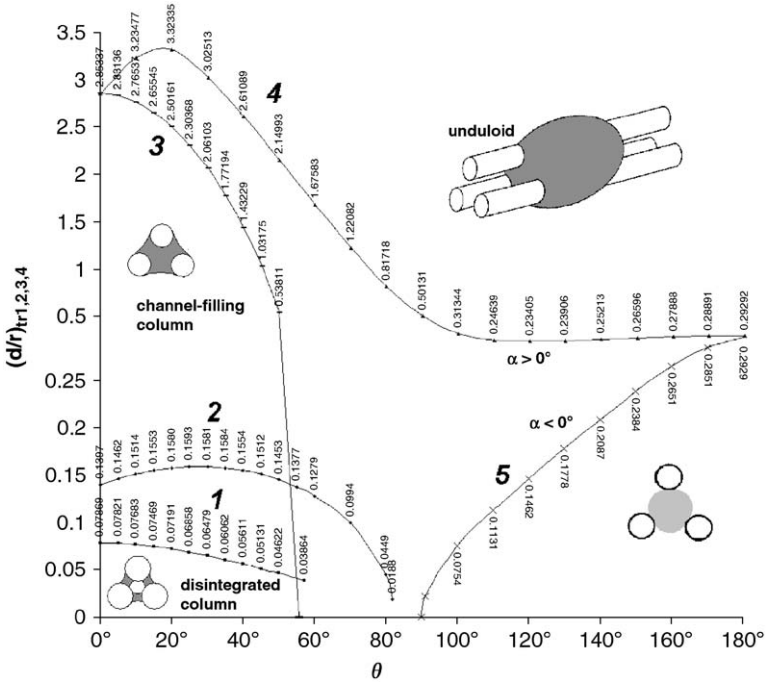

Fig. 12. The morphology diagram for three-cylinder systems. The curve (1) describes the transition from channel-filling columns to disintegrated ones. The points marked by triangles on the curve (2) denote the reversed transition from disintegrated columns to channel-filling columns. The transition from channel-filling column to the "unduloid" is described by the curve (3), while the last $(d/r)'_{tr4}$–θ relationship denotes the morphology transition from the "unduloid" to the channel-filling column with points (4). Curves (3) and (4) are plotted for $S = 0$. Stable columns for $\theta > 90^\circ$ belong to the curve (5), while unstable ones to the curve (4), viz. Fig. 8d. The scale of the $(d/r)'_{tr}$ axis is divided into two parts with different unit lengths. The first ranges from 0 to 0.2 is more detailed while the second has a less minute scale.

The threshold values $(d/r)'_{tr2}$ for filling the central hole can be obtained from Equation (24) by substituting both $\alpha = 30^\circ$ and a chosen contact angle θ or $\sum$ The zero contact angle together with the condition $S = 0$ means we are dealing with the transition from partial wetting to complete wetting just now, provides the threshold value $(d/r)'_{tr2,\ S=0} = 0.13972$. The corresponding transition curve no. 2 is drawn in Fig. 11 as the morphology diagram, together with the $(d/r)'_{tr1}$–θ relationship.

3.3. Transition from the channel-filling column to an unduloid in three-cylinder system

Another stable state of the wetting phase among three cylinders is akin to the unduloid. When the cylinder–cylinder distance exceeds a certain value, the long liquid column disintegrated into unduloids as the only equilibrium configuration. The reason for this second kind of morphological transition in the system in question is based on the fact that the upper limit of α in three-cylinder case is 150°, as a larger covering angle α would require overlap of the two liquid surfaces in contact with each of the cylinder. Corresponding transition values $(d/r)'_{tr3}$ result from Equation (24) by substituting $\alpha = 150^\circ$ and a chosen value of the contact angle θ. Considering zero contact angle and concurrently zero spreading coefficient, we obtain from Eq. (25) the threshold value $\left(d/r\right)'_{tr3,S=0} = \sqrt{3} + 3/\sqrt{2} - 1 \cong 2.85337$. This transition sets in when the distance between three cylinders with channel-filling column, which is originally below $(d/r)'_{tr3}$, increases.

Another transition value $(d/r)'_{tr4}$ occurs when the distance between three cylinders with an "unduloid", i.e., the original distance among the cylinders is greater than $(d/r)'_{tr4}$, reduces. This threshold $(d/r)'_{tr4}$ can be derived from the assumption that the transitional liquid morphology has perfectly circular cross-section with cylinders touching the liquid from the inside.

Owing to the simple cylinder symmetry of the liquid body, Eq. (2) reduces into a simple form that is the equivalent of Eq. (27) for three-cylinder bundle:

$$3 \times 2\pi r\gamma_{SV} = 3 \times 2\pi r\gamma_{SL} + 2\pi R\gamma - \left(\pi R^2 - 3\pi r^2\right)\frac{\gamma}{R}. \tag{33}$$

Note the negative value of the liquid surface radius R for convex liquid body. The third term on the RHS of Eq. (33) is due to the Laplace pressure that acts, for convex surfaces, outward of the liquid. Using again the Young equation $\gamma_{SV} = \gamma_{SL} + \gamma\cos\theta$ one obtains from Eq. (33)

$$\left(\frac{R}{r}\right)'^2 + 6\cos\theta\left(\frac{R}{r}\right)' + 3 = 0. \tag{34}$$

Solutions of this quadratic equation are $\left(R/r\right)'_{1,2} = -3\cos\theta \pm \sqrt{9\cos^2\theta - 3}$. Hence from the minimal value required for $|R| > r + 2r/\sqrt{3}$, we exclude the solution with positive root term and obtain the relation between $(d/r)'_{\mathrm{tr4}}$ and θ under which an unduloid to a channel-filling column transition takes place. Similar to the derivation of Eq. (28) from Eq. (27) we postulate here the liquid column has the shape of the ideal cylinder that touches outer points of the bundle of three solid cylinders. From Eqs. (1) and (34), we have

$$\left(\frac{d}{r}\right)'_{tr4} = \left(3\cos\theta + \sqrt{9\cos^2\theta - 3}\right)\cos\left(\theta + \frac{5\pi}{6}\right) - \frac{\sqrt{3}+2}{2}. \tag{35}$$

Both zero contact angle θ and zero spreading coefficient S lead to the resultant value $(d/r)'_{tr4,\ S=0} = \sqrt{3} + 3/\sqrt{2} - 1 = 2.85337$, which is the same as $(d/r)'_{tr3}$ for the zero contact angle θ and $S = 0$. The corresponding transition curves nos.3 and 4 for $(d/r)'_{\mathrm{tr3}}$ and $(d/r)'_{\mathrm{tr4}}$ are shown in Fig. 12.

For a complete wetting area with $\theta = 0^\circ$ and $S \geq 0$ the term $\cos\theta$ in Eq. (35) has to be substituted by $\sum$ providing us with the relation

$$\left(\frac{d}{r}\right)'_{tr4,CW} = \left(3\Sigma + \sqrt{9\Sigma^2 - 3}\right)\frac{\sqrt{3}}{2} - \frac{\sqrt{3}+2}{2}. \tag{35CW}$$

There exists a great gap between transition curves nos. 3 and 4 in Fig. 12. A channel-filling column cannot be created from an unduloid for contact angles higher than about 54° via drawing solid cylinders nearer to each other, as is visible from curve no. 3. On the other had such a rode-like channel-filling column can be created when the liquid body starts to be fed from inside, for instance by the injection of liquid into the space among a triplet of cylinders, and it remains to be trapped among them like in a birdcage even up to great values of the contact angle, as is obvious from the shape of the curves no. 4 and no. 5. The curve no. 5 is plotted using Eq. (24) for $\alpha < 0^\circ$ and $\theta > 90$.

The last described configuration of thinly spread completely non wetting liquid along the solid substrate is quite unusual and deserves next investigation with another theoretical tools than those used in this work. Of primary importance should be the stability of such configuration. According to Figs. 8c and d it is obvious that stable as well as unstable long liquid columns exist for super-hydrophobic surfaces of cylinders. Stable are those which cowering angle α values less than 0°.

4. Experimental verifications

To validate our theoretical results, we have conducted a series of experiments for both two- and three-cylinder systems. Polypropylene rods of radius 1.5 mm were chosen as the cylinders to meet the requirements of smooth and homogenous surface. Moreover their radius is small enough to minimize the effects of the gravity. A two-component epoxy resin consisting of a mixture of alkylenpolyamids was chosen as the liquid. The time necessary for the resin to solidify is 48 h. So the employment of the resin enabled us to thoroughly examine the sample systems after the resin solidified, as well as to adjust the viscosity and contact angle by altering the resin compositions.

To ensure the equal distances between neighboring pairs of cylinders, wires of certain radii d were used, and arranged into a rose of angles of 120°. These roses were fastened on a glass base. The straws were then located

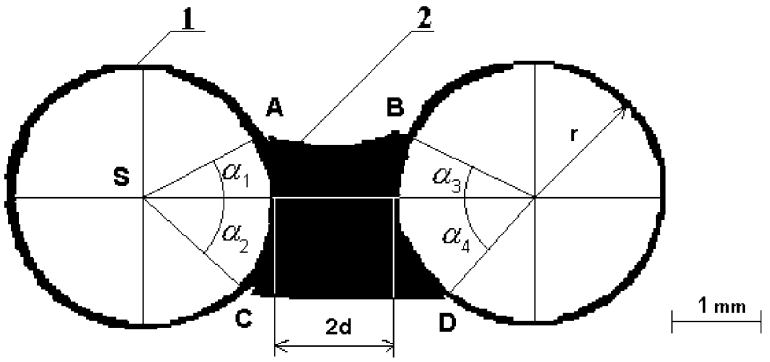

Fig. 13. The cross-section of the two straw systems with solidified resin between them. The straw (1) radius is denoted by r. The distance between straws is $2d$. The long column of resin (2) creates the triplet points A, B, C, and D that provide us with four angles α_1, α_2, α_3, α_4 the average of which is taken as the estimation of the covering angle α.

perpendicular to this bed close to the wire rose by their lower edges. Hence the distance $2d$ between cylinders was secured.

To further minimize the gravitational effects the glass base with the cylinders and applied resin was turned into horizontal position and slowly rotated all around the cylinder bound axis via a special apparatus during resin setting. Once the resin becomes hardened, the cylinder systems with "frozen" liquid columns were examined using a stereo-microscope with digital imaging system for angles and distances. We have prepared and examined more than 150 samples in this study.

A result for two-cylinder system with the "frozen" liquid processed by image analysis is shown in Fig. 13. The measured parameters include: the cylinder–cylinder separation $2d$, fiber radii r, wetting angles θ, and the covering angle α. Resultant values based on these measurements were utilized in constructing d/r–α graphs as shown in Fig. 14 for contact angles $\theta = 45^\circ$, and $\theta = 25^\circ$, respectively. The points represent the experimental data with standard deviations σ for the angle α and distance d, in comparison with the theoretical prediction in solid lines. It is obvious from Fig. 13 that gravity still affected the measurements of angles α because angles α_1 and α_2 in Fig. 13 were systematically larger than α_3 and α_4. To bypass this deviation from the theoretical assumption, we took the average values of all these four α's in plotting Fig. 14, and calculated the standard deviations for particular measurement using these four angles. So a general consistency is shown in between the experiment data and the predictions in both Fig. 14(a) for $\theta = 45^\circ$ and Fig. 14(b) for $\theta = 25^\circ$.

Systems composed of three cylinders were investigated with respect to the transition between split and channel-filling liquid columns. The distance $2d$, diameter $2r$, and the appearance of the hole in the center of the systems as shown in Fig. 15 were our main interests. All experiments have been done for various d/r values at the interval of contact angles within 25° and 45°.

The experimental data are then incorporated into the morphology diagrams in Fig. 16. An empty circle denotes the hole in the center due to the liquid-column disintegration while a filled one denotes the existence of the channel-filling liquid column. The predicted transition curves for $(d/r)'_{tr1}$, and $(d/r)'_{tr2}$ are plotted by solid lines. We can see in the Fig. 16(a) that the disintegration empty circles appeared mostly below the transition curve $(d/r)'_{tr1}$ (Line 1), and rarely between $(d/r)'_{tr1}$ (Line 1) and $(d/r)'_{tr2}$ (Line 2), never above the $(d/r)'_{tr2}$ (Line 2), validating nicely the predictions by the theory. On the other hand however, experimental channel-filling columns occurred even under the transition curve $(d/r)'_{tr1}$ (Line 1) as shown in Fig. 15(b), which is actually forbidden by the theory!

All the contact angle θ values 25°, 30°, 35°, 40°, and 45° used in plotting Fig. 16 were experimentally determined as shown in Fig. 17. A rod was perpendicularly plunged into the resin and the contact angle was measured directly by constructing a tangent line to the liquid surface in the triplet (liquid, solid, and air) point.

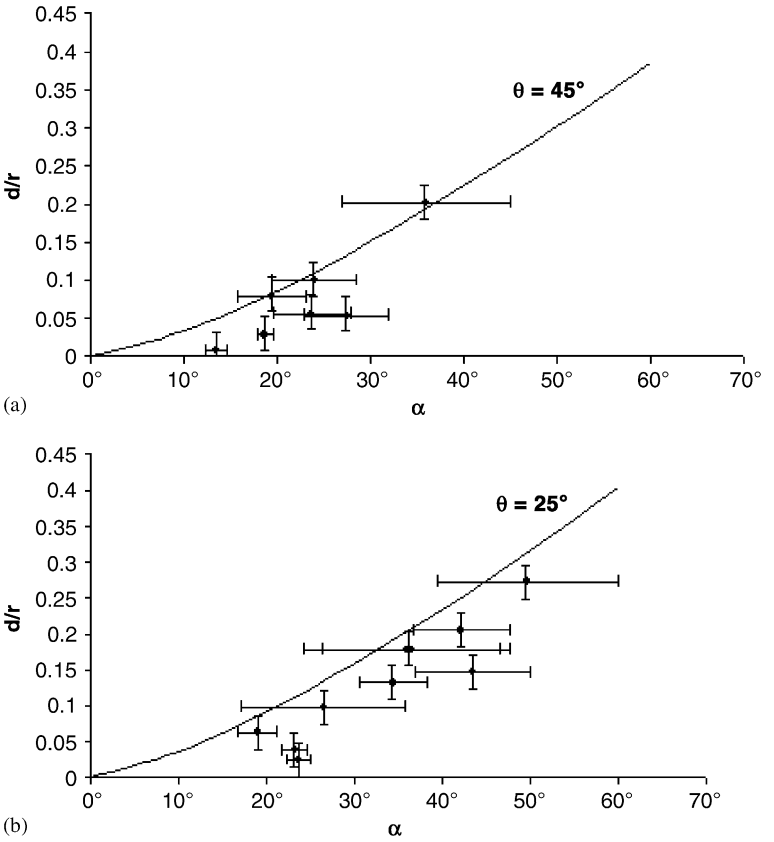

Fig. 14. Experimental data for the relationships between the dimensionless distance (d/r) on the covering angle α in two-straw systems are plotted with their standard deviations σ. The solid lines plot curves predicted by the theory. Fig. 14(a) is for the contact angle $\theta = 45^\circ$, while Fig. 14(b) depicted the relationship for $\theta = 25^\circ$.

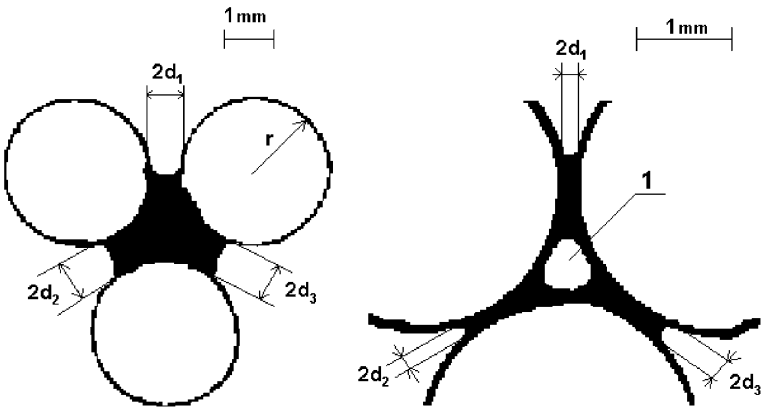

Fig. 15. The cross-sections of two three-straw systems with the solidified resin among them. The left part of the figure represents the channel-filling columns, while the right hand side belongs to the disintegrated ones. The straw–straw separation $2d$ from each experiment was obtained as the average value of three measurements of d_1, d_2, and d_3.

5. Concluding remarks

We have investigated the transitional wetting phenomenon occurring for both two, and three equidistant, parallel cylinders. As opposed to Princen's works [1–3] we extended our analysis to the complete wetting

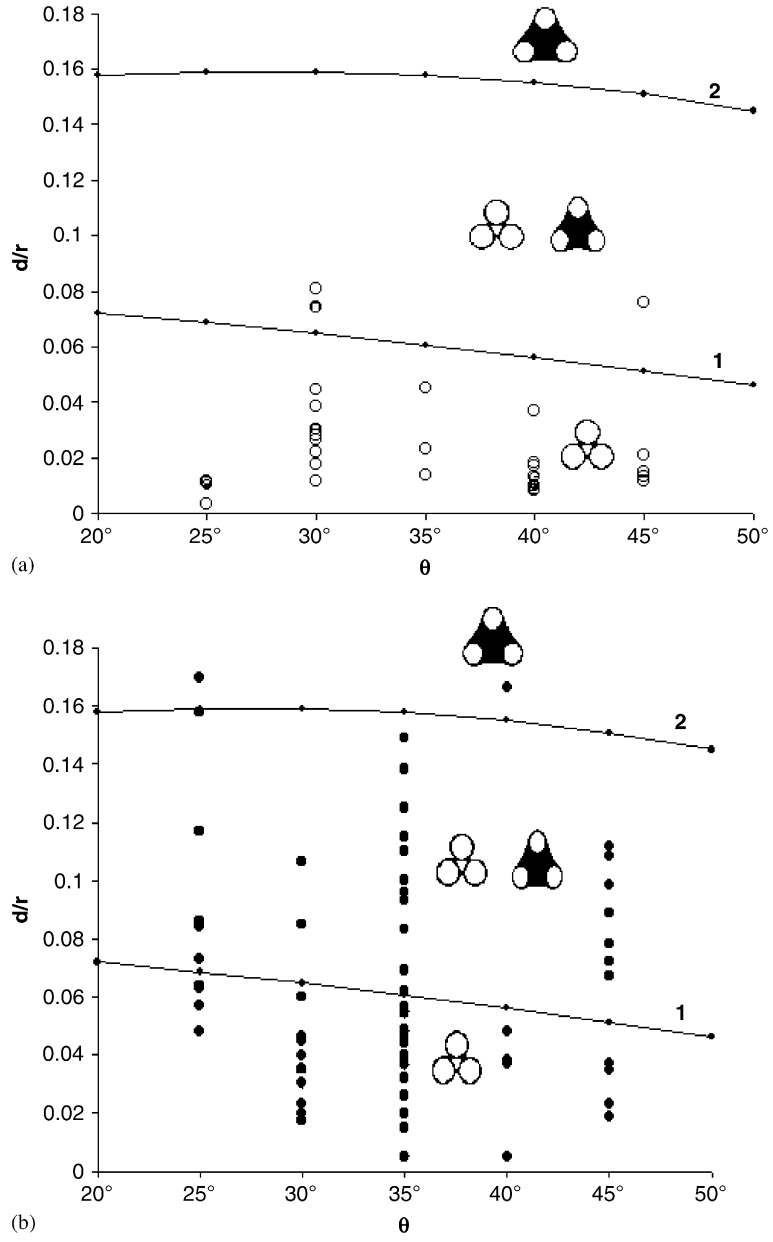

Fig. 16. Morphology diagrams of the transitions between disintegrated column and channel-filling column. These threshold values of d/r are denoted in the theory as $(d/r)'_{tr1}$ (the curve no. 1), and $(d/r)'_{tr2}$ (the curve no. 2). The empty circles in Fig. 16(a) reflect the disintegrated columns, whereas the filled points in Fig. 16(b) represent the channel-filling columns. The investigated interval of contact angles θ ranges from 25° to 45°.

instances, where $S>0$, and to the hypothetic situations $S<-2\gamma$. We have shown that unstable long liquid columns, in the regime of super-hydrophobicity, can exist theoretically even between pairs of parallel cylinders. The three-cylinder systems in this "completely non wetting" area exhibit both unstable and stable long liquid columns.

We have shown that a number of different morphologies of the wetting phase are possible. For instance for two-cylinder systems, liquid columns and unduloids are the only two alternatives; whereas three

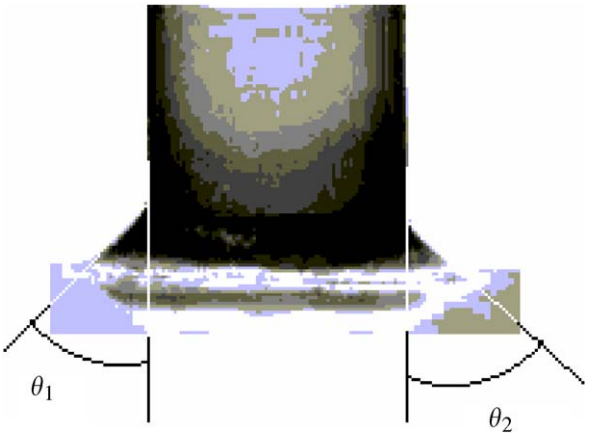

Fig. 17. The image of the straw partly plunged into the resin. This kind of images was used for the measurements of contact angles θ. Two contact angles θ_1 and θ_2 can be obtained from each image and averaged to give θ.

morphologies, multiple liquid columns, channel-filling column and unduloids, can be observed for the three-cylinder systems. With the theory developed in this work, we are able to predict the morphological transitions processes between different types of liquid columns and unduloids. All transition curves predicted in morphology diagrams exhibit transition hysteresis.

Our experiments provided data to verify our predictions. We focused on the dependence of the covering angle α on the dimensionless cylinder–cylinder distance d/r for systems composed of two-cylinders, and transition of the channel-filling liquid column to split columns for three-cylinder systems. The experimental data show consistency with the predictions on the morphological transitions, except in the case of channel-filling columns. This discrepancy can be attributed to the sensitivity of the experiments to impurities and alignment of cylinders that are supposed to be perfectly parallel with each other. We contemplate next to carry out a Monte Carlo simulation, based for instance on our works [10–13], to demonstrate the existence of transition hysteresis.

Acknowledgement

Lukáš, Chaloupek, and Košťáková would like to express their thanks to The Ministry of Education of the Czech Republic for the support of this work from the project CEP1-1M0554 in the frame of The Research Center for Advanced Conservation Technologies.

References

[1] H.M. Princen, Capillary Phenomena in assemblies of Parallel Cylinders: Capillary Rise between Two Cylinders, J. Colloid Interface Sci. 30 (1969) 69.
[2] H.M. Princen, Capillary Phenomena in Assemblies of parallel Cylinders: II. Capillary Rise in Systems with More Than Two Cylinders, J. Colloid Interface Sci. 30 (1969) 359.
[3] H.M. Princen, Capillary Phenomena in Assemblies of Parallel Cylinders: III. Liquid Columns between Horizontal Parallel Cylinders, J. Colloid Interface Sci. 34 (1970) 171.
[4] P.-G. de Gennes, F.D. Wyart-Brochard, D. Quere, Capillarity and Wetting Phenomena; Drops, Bubbles, Pearls, Waves, Springer, New York, Berlin, 2003.
[5] P. Lenz, R. Lipowsky, Morphological Transitions of Wetting Layers on Structured Surfaces, Phys. Rev. Lett. 80 (1998) 1920.
[6] Ryong-Joon Roe, Wetting of Fine Wires and Films by a Liquid Film, J. Colloid Interface Sci. 50 (1975) 70.
[7] H. Gau, S. Herminghaus, P. Lenz, R. Lipowsky, Liquid Morphologies on Structured Surfaces: From Microchannels to Microchips, Science 283 (1999) 46.
[8] P.S. Swain, R. Lipowsky, Wetting between Structured Surfaces: Liquid Bridges and Induced Forces, Europhys. Lett 49 (2000) 203.
[9] A.W. Adamson, A.T. Gast, Physical Chemistry of Surfaces, Wiley, New York, 1997.

[10] B.J. Carroll, Equilibrium Conformations of Liquid Drops on Thin Cylinders under Forces of Capillarity: A Theory for the Roll-up Process, Langmuir 2 (1985) 248.
[11] D. Lukas, E. Glazyrina, N. Pan, Computer Simulation of Liquid Wetting Dynamics in Fiber Structures Using the Ising Model, J. Text. Inst. 88 (1997) 149.
[12] D. Lukas, N. Pan, Wetting of a Fiber Bundle in Fibrous Structures, Polymer Composites 24 (2003) 314.
[13] D. Lukas, V. Soukupova, N. PAN, Computer Simulation of 3-D Liquid Transport in Fibrous Materials, Simulation 80 (2004) 547.